Blue luminescence from Ce-doped ZnO thin films prepared by magnetron sputtering

Q. Luo · L.S. Wang · H.Z. Guo · K.Q. Lin · Y. Chen · G.H. Yue · D.L. Peng

Abstract The photoluminescence properties of undoped and Ce-doped ZnO thin films that were prepared by DC magnetron sputtering were investigated. It was found that the incorporation of Ce could intensively affect the structural, optical, and photoluminescence properties of the ZnO thin films. The undoped ZnO thin films showed a sharp UV luminescence, whereas the Ce-doped ZnO thin films showed a broad blue luminescence. The effects of excitation wavelength and annealing atmosphere on the photoluminescence properties of Ce-doped ZnO thin films were also studied. After post-annealing in air and oxygen atmospheres, the blue emissions of the prepared films were drastically suppressed. Our results indicate that the blue emissions of Ce-doped ZnO thin films are related to zinc interstitials and the intrinsic transition of Ce^{3+} ions.

1 Introduction

ZnO is well known as a promising optoelectronic material with a wide band gap of 3.37 eV at room temperature, large exciton binding energy of 60 meV, and easy growth at low cost [1]. When ZnO is excited by ultraviolet light, it can emit UV, violet, blue, green, and yellow light [2–5]. The blue luminescence of ZnO has great potential applications in the field of visible-light-emitting devices and biological fluorescence labeling [6, 7]. The extrinsic doping can greatly influence the optical and photoluminescence properties of ZnO. Ce is a major element which

has excellent luminescent properties when doped into matrix materials. As a dopant, Ce has received great attention due to its peculiar optical and catalytic properties arising from the availability of the shielded 4f levels [8]. The emission from Ce^{3+} is in either the UV or the visible region [9]. Thus, Ce-doped ZnO nanomaterial may be expected to be a potential candidate material for photoluminescence devices. In recent years, Ce-doped ZnO nanostructures, such as nanoparticles, nanotubes, nanowires, and nanorods, have been prepared by many synthetic routes such as the sonochemical wet-impregnation method [10], the electrochemical route [11], spray pyrolysis [12], chemical vapor reaction [13], etc. However, up to now, studies of the photoluminescence properties have been done mainly on Ce-doped ZnO one-dimensional nanostructures, and there is little work concerning the preparation and photoluminescence properties of Ce-doped ZnO thin films.

In this paper, undoped ZnO and Ce-doped ZnO thin films were prepared by DC magnetron sputtering. Three blue emissions were observed from the Ce-doped ZnO thin films. Detailed and systematic investigations of photoluminescence properties of the Ce-doped ZnO thin films were carried out under different annealing atmospheres, such as nitrogen, air, and oxygen. Here, we focused on the luminescence origin and mechanism of Ce-doped ZnO thin films and compared them with undoped ZnO thin films. Our results demonstrate a great promise for changing the transitions in ZnO films with potential applications in optoelectronic devices.

Q. Luo · L.S. Wang · H.Z. Guo · K.Q. Lin · Y. Chen · G.H. Yue ·
D.L. Peng (✉)
Department of Materials Science and Engineering, College
of Materials, Xiamen University, Xiamen 361005, P.R. China
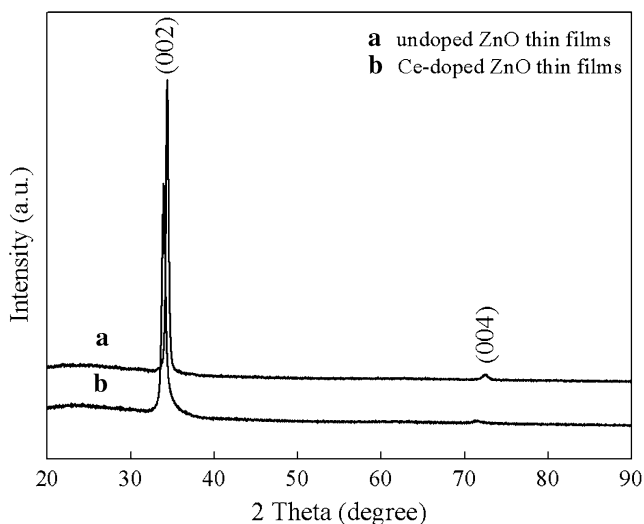e-mail: dlpeng@xmu.edu.cn
Fax: +86-592-2180155

2 Experimental

Undoped ZnO and Ce-doped ZnO thin films were deposited on glass substrates by a DC reactive magnetron sputtering

Fig. 1 XRD patterns of undoped and Ce-doped ZnO thin films

technique using a pure Zn (99.99 %) metallic target and a pure $Zn_{97}Ce_3$ (99.99 %) alloy target in high-purity oxygen and argon gas atmosphere. All substrates were ultrasonically cleaned with acetone and absolute alcohol for 15 min, respectively, and then dried by nitrogen. The substrate holder with a rotational speed of 30 rpm was mounted in the upper part of the chamber. The target-to-substrate distance is about 80 mm. The chamber was pumped to a base pressure of 4.0×10^{-4} Pa and film growth was carried out in a growth ambient with $Ar/O_2 (7:3)$ mixture gas of 24 sccm at a working pressure of 0.6 Pa and a constant power of 150 W. All the samples were deposited for 40 min. The Ce-doped ZnO thin films were annealed in nitrogen, air, and oxygen, respectively at a temperature of 600 °C for 1 h.

The crystalline structures of the Ce-doped ZnO thin films were investigated by X-ray diffraction (XRD, Panalytical X'pert-PRO) using Cu K_α radiation. The surface morphology was analyzed by a scanning electron microscope (SEM, LEO-1530FE). X-ray photoelectron spectroscopy (XPS) was carried out using a PHI Quantum 2000 scanning ESCA microprobe instrument. UV-Vis absorption spectra were recorded on a Varian Cary 5000 recording spectrometer. Photoluminescence (PL) and PL excitation (PLE) spectra were measured using a Hitachi F7000 fluorescence spectrophotometer equipped with a 150-W Xe lamp as the excitation source. All measurements were carried out at room temperature.

3 Results and discussion

Figure 1 displays the typical XRD patterns of undoped ZnO and Ce-doped ZnO thin films. The strong (002) and weak (004) peaks can be indexed to a hexagonal wurtzite ZnO structure, which implies the preferential c-axis orientation
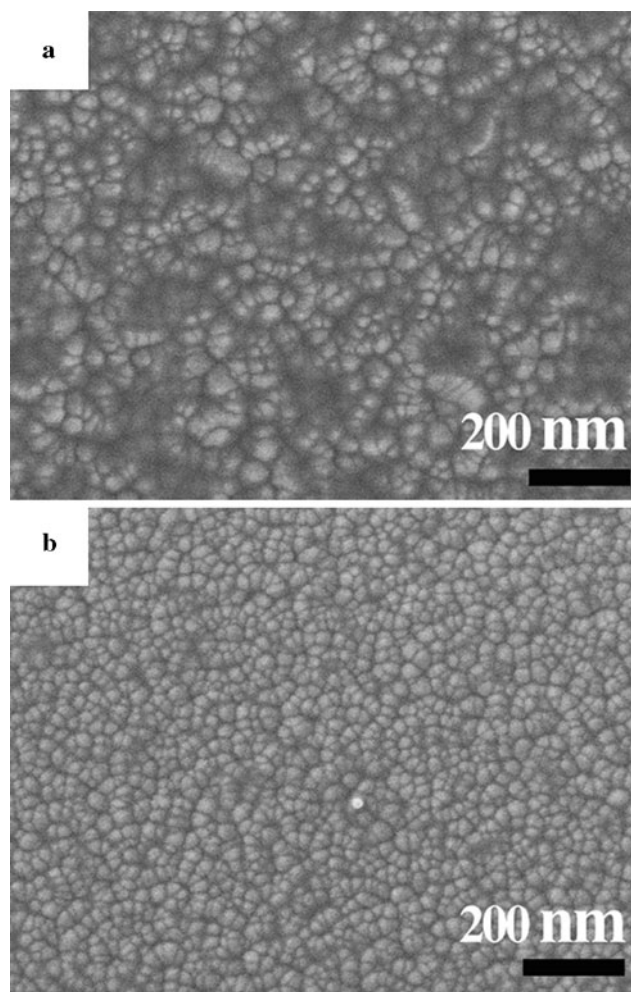

Fig. 2 SEM images of undoped (**a**) and Ce-doped (**b**) ZnO thin films

due to the lowest surface free energy of the (002) plane [14]. No diffraction peaks of Ce, CeO_2, or Ce_2O_3 phases were observed in our samples. The (002) peak positions of undoped and Ce-doped ZnO thin films are located at $2\theta = 34.43$ and 33.91°, respectively. Compared with the (002) peak position of ZnO powder diffraction at 34.45° (see JCPDS file no. 36-1451), the diffraction pattern of Ce-doped samples shifts slightly toward lower angles while the undoped samples are nearly unchanged, which indicates that the Ce ion are incorporated into the ZnO crystal lattice and substitute for the Zn^{2+} sites. The lower angle shift of the XRD peaks of Ce-doped ZnO thin films can be explained as follows. When Ce ions substitute into the Zn^{2+} sites in the ZnO lattice, the lattice parameters will be slightly increased due to the bigger radius of Ce^{3+} ions (1.15 Å) compared to Zn^{2+} ions (0.74 Å), which will shift the ZnO (002) peak to lower angles. Figure 2 shows the SEM images of undoped (a) and Ce-doped (b) ZnO thin films. It can be noted that Ce doping has an influence on film surface morphology. The grain size of ZnO thin films decreases after Ce doping. The morphology of the grains is found to be uniform and dense.
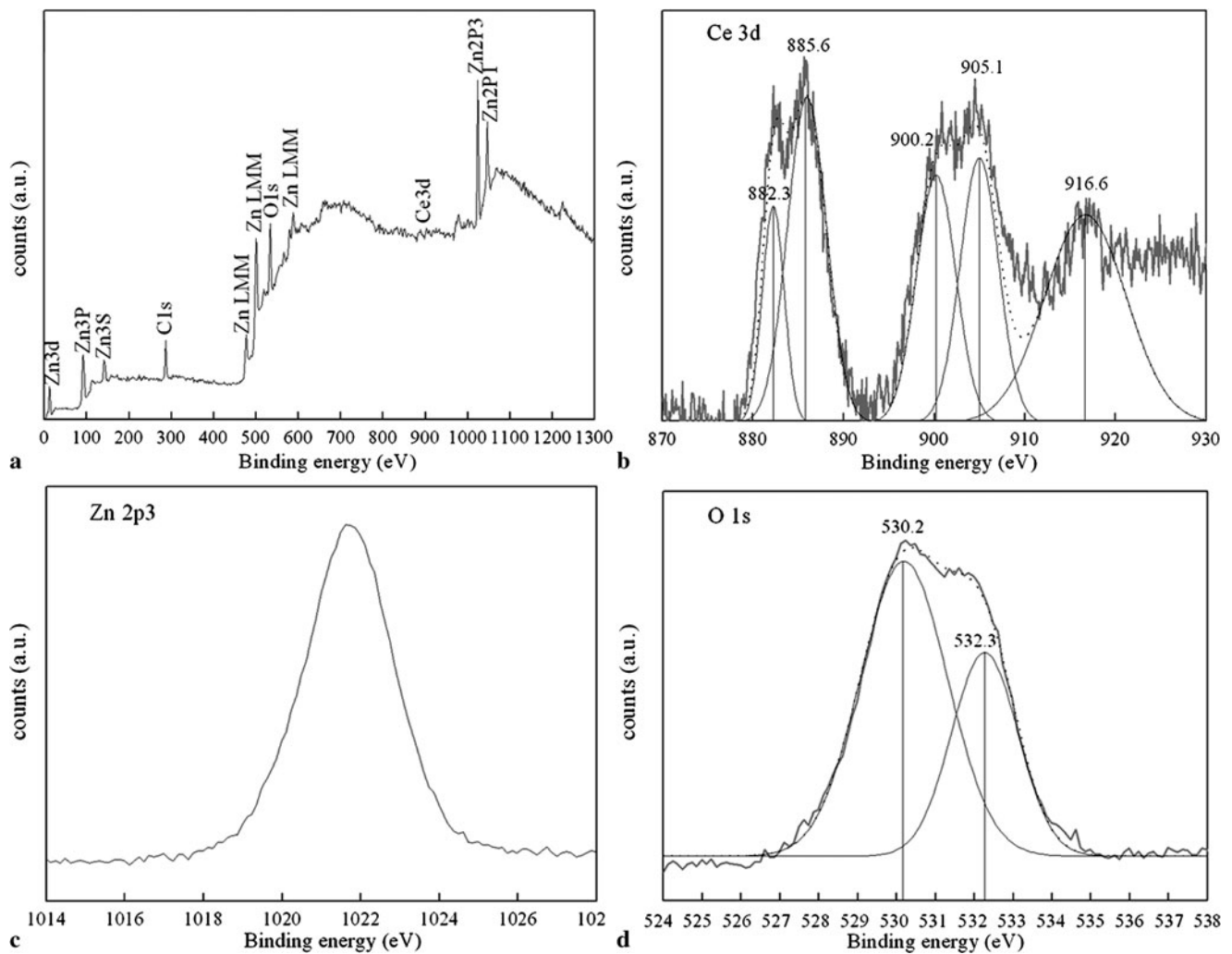
Fig. 3 XPS spectra of Ce-doped ZnO thin films and high-resolution scans of Ce 3d, Zn 2p, and O 1s peaks

Figure 3 shows the XPS spectra of the Ce-doped ZnO thin films and the high-resolution scans of Ce 3d, Zn 2p, and O 1s peaks. All the XPS spectra were corrected for specimen charging by referencing the C 1s peak to 284.60 eV. The Zn $2p_{3/2}$ peak was symmetric and centered at 1021.7 eV, which can be attributed to the formation of Zn^{2+} in the ZnO lattice [15]. The O 1s spectrum was fitted with two components. The low-energy component at 530.2 eV is associated to the Zn–O bond in the ZnO thin film. The high-energy component at 532.3 eV is related to oxygen species chemisorbed at the surface [16]. The high-resolution scans (Fig. 3b) show that the binding energy of Ce 3d is located at 882.3, 885.6, 900.2, 905.1, and 916.6 eV. The characteristic peak at 885.6 eV indicates that Ce^{3+} exists in Ce-doped ZnO thin films [17]. The peaks occurring at 882.3, 905.1, and 916.6 eV of the binding energy exist in the transition of Ce^{4+} between energy levels [18]. The characteristic peak at 883.8 eV of zero-valent cerium was not observed in our Ce 3d spectra [19]. The cerium content was determined to be

1.12 % by calculating the peak areas. These results indicate that Ce^{3+} and Ce^{4+} ions coexist in our samples.

The effect of Ce on the optical properties of ZnO thin films has been studied. Figure 4 shows the transmittance spectra of undoped and Ce-doped ZnO thin films; the inset is the plot of $(\alpha h\nu)^2$ versus $h\nu$. It can be noticed that all the samples have high transparency in the visible range and have a strong absorption near the band edge of ZnO. Compared with undoped ZnO thin films, the optical absorption edge of Ce-doped ZnO thin films has a blue shift to the region of higher photon energy. When Ce atoms are incorporated into ZnO, a lot of Ce^{3+} and Ce^{4+} ions and zinc interstitials are formed. Ce^{3+} and Ce^{4+} ions on substitutional sites of Zn^{2+} ions and Ce interstitial atoms increase the carrier concentration. The effect of absorption-edge shift with increasing carrier concentration is attributed to the well-known Burstein–Moss (BM) effect [20]. Ce-doped ZnO is a natural n-type semiconductor material, and the Fermi level will move to the bottom of or above the conduction band when the increasing
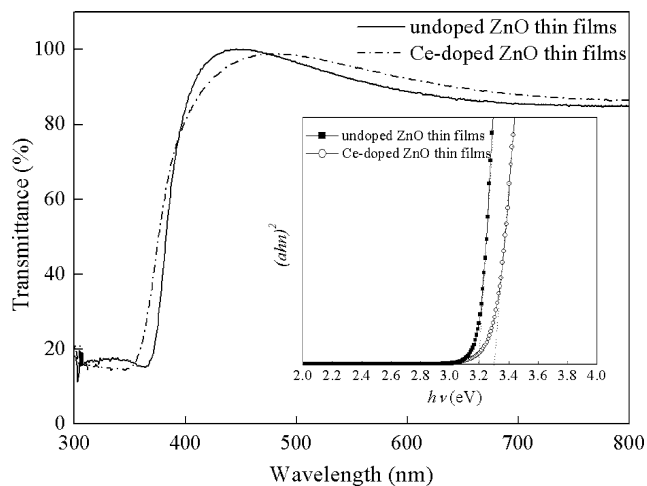
Fig. 4 Transmittance spectra of undoped and Ce-doped ZnO thin films

Fig. 5 Photoluminescence emission spectra of undoped (**a**) and Ce-doped (**b**) ZnO thin films

carriers fill in the conduction band. Therefore, the distance of electron vertical transitions from the valence band to the conduction band is increased. The BM shift (ΔE_{BM}) of the band-edge absorption in the n-type semiconductor is given as [21]

$$\Delta E_{BM} = \left[1 + (m_e^*)/(m_h^*)\right] \\ \times \left[\left(\frac{3}{\pi}\right)^{2/3} (h^2)/(8m_e^*)n^{2/3} - 4kT\right]. \quad (1)$$

In this equation, h, k, T, n, m_e^*, and m_h^* refer to Planck's constant, Boltzmann's constant, absolute temperature, electron carrier concentration in the conduction band, effective mass of electrons, and effective mass of holes, respectively. According to this equation, the optical gap band is widened with the carrier concentration increasing. We also calculate the energy gap E_g. The value of E_g can be determined by using the band to band absorption given by [22]

$$\alpha h\nu = A(h\nu - E_g), \quad (2)$$

where A, E_g, and $h\nu$ represent a constant, the band gap, and the incident photon energy, respectively. The energy gap is determined from the extrapolation of the linear part of the $(\alpha h\nu)^2$ versus $h\nu$ plot. The band gap increases from 3.19 eV for undoped ZnO films to 3.29 eV for Ce-doped ZnO thin films.

Figure 5 presents the room-temperature PL spectra of the ZnO thin films with and without Ce incorporation. The PL spectrum of undoped ZnO thin films excited by a wavelength of 325 nm is composed of an ultraviolet-band peak at 394 nm, which is the characteristic PL peak. For undoped ZnO, an electron in the valence band can be excited to the conduction band when the energy of a photon is equal to or higher than the band gap. The UV emission is attributed to the recombination of the photoexcited holes and the electrons via a radiative process. We performed a Gaussian peak
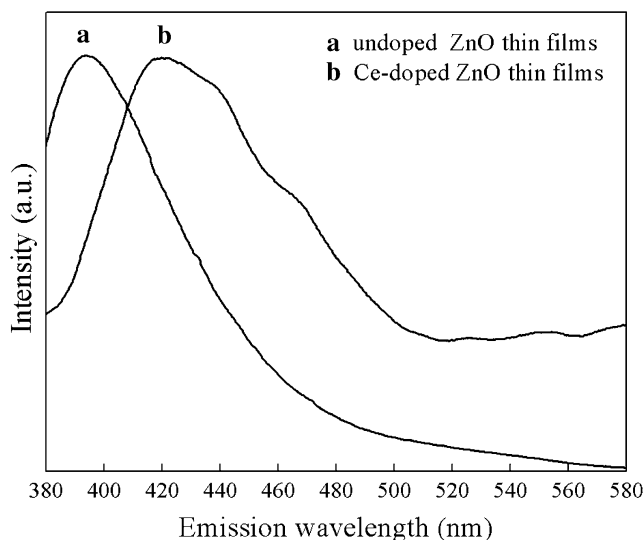
fitting of the PL spectrum of Ce-doped ZnO thin films using a linear least square method. Three main peaks at 418, 441, and 463 nm were identified. Koao et al. [23] observed two peaks at 422 and 450 nm, which were ascribed to the electric-dipole-allowed transition of the Ce^{3+} ions. The following reactions would spontaneously occur during the deposition of Ce-doped ZnO thin films:

$$2Ce + 3ZnO \rightarrow Ce_2O_3 + 3Zn + 3V_O, \quad (3)$$

$$2Ce + 3ZnO \rightarrow Ce_2O_3 + 3Zn_i. \quad (4)$$
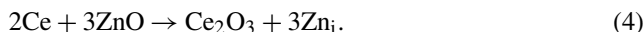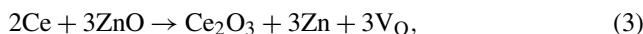
When a Ce atom was incorporated into ZnO, it would take oxygen from the ZnO and form V_O, Zn_i, and Ce^{3+} ions. Zinc interstitials and oxygen vacancies are known to be the predominant ionic defect types [24]. The zinc interstitials come from the Frenkel reaction, while the oxygen vacancies come from the Schottky reaction. In our experiment, the temperature of the substrate can only reach 200–300 °C under the zinc-ion bombardment, where Frenkel defects predominate. So, it is possible to assume that the zinc interstitials are the predominant donor defects, while the oxygen vacancies are probably existing in a small amount. Zeng et al. [25] observed a dominant blue emission at 440 nm, which was attributed to the transitions involving zinc interstitials. When the Ce^{3+} ions are incorporated into ZnO, the band-gap structure of ZnO will be modulated substantially and new multi-emission centers are formed, such as the emission of the impurity level to the valence band, and the intrinsic transition of Ce^{3+} ions [26, 27]. Therefore, the blue emissions could be related to the Ce^{3+} ions and the zinc interstitials in ZnO.

Ce-doped ZnO thin films were excited at various wavelengths and further annealed in different atmospheres to investigate the detailed mechanism of these emissions. Figure 6 presents the excitation-dependent PL (ED-PL) spectra
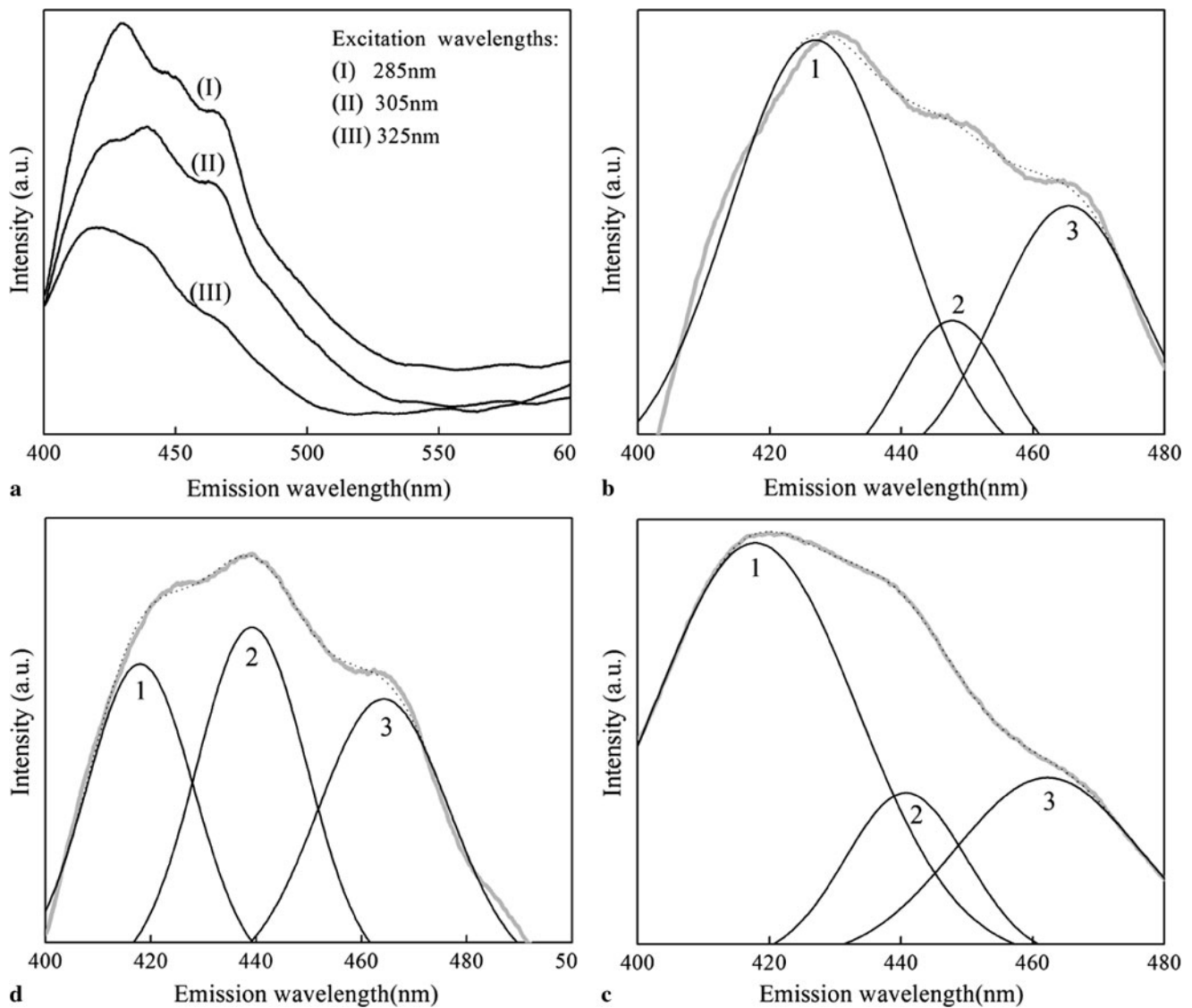
Fig. 6 (**a**) ED-PL spectra of Ce-doped ZnO thin films obtained at different excitation wavelengths. (**b**), (**c**), and (**d**) are the Gaussian curve fits for the spectra *I*, *II*, and *III* in (**a**), respectively

and the Gaussian curve fits for the ED-PL spectra of the Ce-doped ZnO thin films. All the spectra show the presence of three main peaks. They are referred to as Peak 1, Peak 2, and Peak 3. The peak positions and peak position differences are tabulated in Table 1. The energy difference between $^2F_{5/2}$ and $^2F_{7/2}$ in Ce^{3+} ions is expected to be about 2000 cm^{-1} [28]. For three excitation wavelengths, the energy differences between Peak 1 and Peak 3 are 1914, 2371, and 2325 cm^{-1}, which are very close to the expected energy difference. The blue emission in Ce^{3+} occurs at 24000 cm^{-1} (417 nm) [29], which is consistent with our results (Peak 1). Therefore, we can conclude that Peak 1 and Peak 3 originate from the transitions from the lower 5d (^2D) excited state to the split $^2F_{5/2}$ and $^2F_{7/2}$ energy levels. Figure 7 depicts the PL spectra of Ce-doped ZnO thin films post-annealed

Table 1 Peak positions and adjacent peak position differences for the curve fitting in Fig. 6

	Peak	Position (nm)	Position (cm^{-1})	Peak position difference (cm^{-1})
Fig. 6b	1	427	23419	–
	3	465	21505	1914
Fig. 6c	1	418	23923	–
	3	464	21552	2371
Fig. 6d	1	418	23923	–
	3	463	21598	2325

at 600 °C in nitrogen, air, and oxygen atmospheres. From the samples post-annealed in a flow of nitrogen, we can ob-
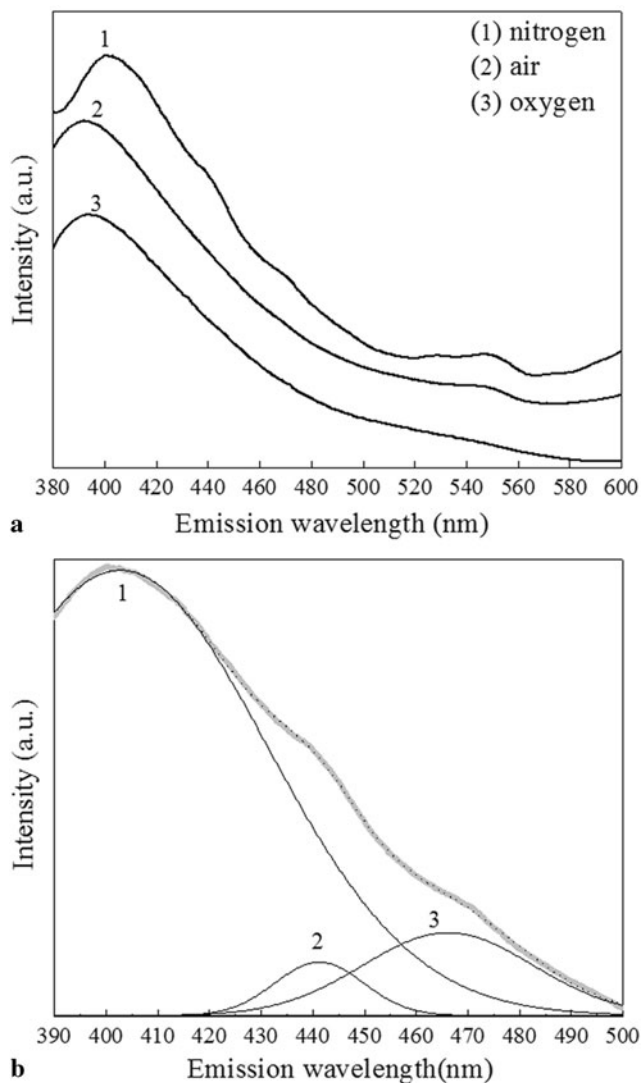
Fig. 7 PL spectra of Ce-doped ZnO thin films post-annealed in different atmospheres (**a**) and Gaussian peak fitting for samples post-annealed in nitrogen (**b**)

Fig. 8 Schematic diagram for the mechanism of the blue emissions of Ce-doped ZnO thin films

serve that the spectrum consists of a dominant UV emission at 403 nm together with two relatively weak blue emission bands at 441 and 467 nm. However, when the samples are post-annealed in air and oxygen atmospheres, the major blue emissions are replaced by the UV emission at around 396 nm. The Ce ions are known to have two main different oxidation states of Ce^{4+} and Ce^{3+}. The Ce^{4+} ions have a strong tendency to attract electrons, while the Ce^{3+} ions easily suffer from oxidation. Under oxidation conditions, once all Ce^{3+} ions are converted into Ce^{4+} ions, transitions between 5d and 4f orbitals become impossible, which leads to the quenching of the two blue emissions at 418 nm (Peak 1) and 463 nm (Peak 3). In addition, when Ce-doped ZnO thin films were annealed at 600 °C in air or oxygen atmosphere, a part of the zinc interstitials would return to the
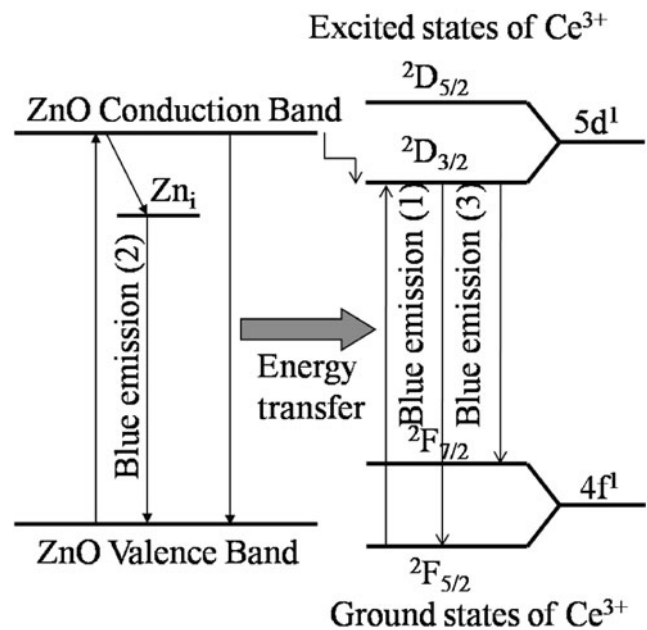
lattice site [30]. Thus, the intensity of the blue emission at 441 nm (Peak 2) is markedly reduced. The above results also suggest that the blue emissions are related to the Ce^{3+} ions and zinc interstitials.

A schematic diagram accounting for the blue emissions of Ce-doped ZnO thin films is drawn (Fig. 8) for better understanding the PL mechanism. When the ZnO hosts absorb energy from the excitation source, the electrons are excited up to the conduction band. Some of the electrons nonradiatively transit into above Zn_i initial states, and then radiatively transit into the valence band. The UV emission band of ZnO is overlapping with the $^2D_{3/2} \rightarrow {}^2F_{5/2}$ absorption lines of Ce^{3+} ions. If the electrons in the conduction band recombine with the holes in the valence band, a part of the recombination energy can be rapidly transferred to the Ce^{3+} ions through a resonant energy transfer process. This process can promote the electrons of Ce^{3+} ions transiting from the ground states to the excited states. In addition, there is another emission process. Energy absorbed by the formation of free charge carriers can be transported through the crystal lattice (diffusion or tunneling process). The charge carriers will be trapped at luminescent centers in the crystal lattice where radiative recombination occurs [31]. As is well known, under the influence of the crystal field, the $5d_1$ excited configuration in Ce^{3+} splits into two components ($^2D_{5/2}$ and $^2D_{3/2}$), and the $4f_1$ ground state configuration yields two components ($^2F_{5/2}$ and $^2F_{7/2}$) due to spin–orbit coupling [32]. The blue emissions originate from the lower 5d excited state to the split $^2F_{5/2}$ and $^2F_{7/2}$ energy levels.

4 Conclusions

Undoped and Ce-doped ZnO thin films were prepared by DC magnetron sputtering and their structural, optical, and luminescent properties were studied. Compared with the un-doped ZnO thin films, the optical absorption edge of the Ce-doped ZnO thin films has a blue shift to the region of higher photon energy. It was found that the incorporation of Ce into ZnO led to the presence of a large number of defects and the formation of new energy levels in the band gap. The blue emissions could originate from the transitions from the Zn_i state to the valence band and $^5d_1 \rightarrow {}^4f_1$ transitions in Ce^{3+} ions. Such Ce-doped ZnO thin films with blue luminescent properties are promising candidates for potential applications in optoelectronic devices.

References

1. A. Bera, T. Ghosh, D. Basak, ACS Appl. Mater. Interfaces **2**, 2895 (2010)
2. F. Leiter, H. Alves, D. Pfisterer, N.G. Romanov, D.M. Hofmann, B.K. Meyer, Physica B **340–342**, 201 (2003)
3. H.B. Zeng, S.K. Yang, X.X. Xu, W.P. Cai, Appl. Phys. Lett. **95**, 191904 (2009)
4. K. Vanheusden, C.H. Seager, W.L. Warren, D.R. Tallant, J.A. Voigt, Appl. Phys. Lett. **68**, 403 (1996)
5. S.A. Studenikin, N. Golego, M. Cocivera, J. Appl. Phys. **84**, 2287 (1998)
6. Y. Masuda, N. Kinoshita, F. Sato, K. Koumoto, Cryst. Growth Des. **6**, 75 (2006)
7. M. Bruchez Jr., M. Moronne, P. Gin, S. Weiss, A.P. Alivisatos, Science **281**, 2013 (1998)
8. L. Liao, H.X. Mai, Q. Yuan, H.B. Lu, J.C. Li, C. Liu, C.H. Yan, Z.X. Shen, T. Yu, J. Phys. Chem. C **112**, 9061 (2008)
9. L.F. Koao, H.C. Swart, F.B. Dejene, J. Rare Earths **28**, 206 (2010)
10. C. Karunakara, P. Gomathisankar, G. Manikandan, Mater. Chem. Phys. **123**, 585 (2010)
11. G.R. Li, X.H. Lu, W.X. Zhao, C.Y. Su, Y.X. Tong, Cryst. Growth Des. **8**, 1276 (2008)
12. Z. Sofiani, B. Derkowska, P. Dalasinski, M. Wojdyła, S. Dabos-Seignon, M. Alaoui Lamrani, L. Dghoughi, W. Bała, M. Addou, B. Sahraoui, Opt. Commun. **267**, 433 (2006)
13. B.C. Cheng, Y.H. Xiao, G.S. Wu, L.D. Zhang, Adv. Funct. Mater. **14**, 913 (2004)
14. K.L. Chapra, S. Major, D.K. Pandya, Thin Solid Films **102**, 1 (1983)
15. M. Yousefi, R. Azimirad, M. Amiri, A.Z. Moshfegh, Thin Solid Films **520**, 721 (2011)
16. M. Yousefi, M. Amiri, R. Azimirad, A.Z. Moshfegh, J. Electroanal. Chem. **661**, 106 (2011)
17. X. Zhang, H.L. Wan, W.Z. Weng, X.D. Yi, J. Mol. Catal. A, Chem. **200**, 291 (2003)
18. F. Li, B. Yan, J. Zhang, A.X. Jiang, C.H. Shao, X.J. Kong, X. Wang, J. Rare Earths **25**, 306 (2007)
19. L. Schlapbach, J. Osterwalder, Solid State Commun. **42**, 271 (1982)
20. M. Suchea, S. Christoulakis, N. Katsarakis, T. Kitsopoulos, G. Kiriakidis, Thin Solid Films **515**, 6562 (2007)
21. Y.G. Chang, J. Xu, Y.Y. Zhang, S.Y. Ma, L.H. Xin, L.N. Zhu, C.T. Xu, J. Phys. Chem. C **113**, 18761 (2009)
22. K. Sivaramakrishnan, T.L. Alford, Appl. Phys. Lett. **94**, 052104 (2009)
23. L.F. Koao, H.C. Swart, E. Coetsee, M.M. Biggs, F.B. Dejene, Physica B **404**, 4499 (2009)
24. K.I. Hagemark, J. Solid State Chem. **16**, 293 (1976)
25. H. Zeng, G. Duan, Y. Li, S. Yang, X. Xu, W. Cai, Adv. Funct. Mater. **20**, 561 (2010)
26. Y.C. Kong, D.P. Yu, B. Zhang, W. Fang, S.Q. Feng, Appl. Phys. Lett. **78**, 407 (2001)
27. W.I. Park, Y.H. Jun, S.W. Jung, G.-C. Yi, Appl. Phys. Lett. **82**, 964 (2003)
28. E. Coetsee, J.J. Terblans, O.M. Ntwaeaborwa, H.C. Swart, Physica B **404**, 4426 (2009)
29. O. Ntwaeaborwa, H. Swart, R. Kroon, P. Holloway, J. Botha, J. Phys. Chem. Solids **67**, 1749 (2006)
30. M. Wang, E.J. Kim, J.S. Chung, E.W. Shin, S.H. Hahn, K.E. Lee, C. Park, Phys. Status Solidi A **203**, 2418 (2006)
31. G. Blasse, B.C. Grabmaier, *Luminescent Materials* (Springer, Berlin, 1994)
32. O.M. Ntwaeaborwa, P.H. Holloway, Nanotechnology **16**, 865 (2005)